Lasers in Manufacturing Conference 2019

Integrated Numerical and Machine Learning Model for Deposition Path Planning in Multi-layer Laser Aided Additive Manufacturing

Y.X. Chew[a], K. Ren[b,] G.J. Bi[a*], Y.F. Zhang[b], J.Y.H. Fuh[b]

[a]*Singapore Institute of Manufacturing Technology, 73 Nanyang Drive, Singapore 637662, Singapore*
[b]*Department of Mechanical Engineering, National University of Singapore, Singapore 117576, Singapore*

Abstract

Laser Aided Additive Manufacturing (LAAM) is a flexible AM process, enabling high build rate via direct metal deposition. Higher build rate with higher laser power input and rapid layer-by-layer deposition will lead to localized heat accumulation. This effect can be minimized by optimizing laser deposition patterns to manage temperature distribution to improve consistency in dimensions and microstructure. A numerical modelling and machine learning approach was developed. The numerical model first generates temperature field data for 8 different raster scan laser deposition patterns for the first few deposition layers to train the Temperature Pattern Recurrent Neural Networks (TP-RNN) machine learning algorithm. Subsequently, the TP-RNN algorithm outputs a simplified temperature field of the next layer for selecting the optimal pattern. The numerical model then computes thermal field of the determined optimized pattern as input data to propagate the analysis to the next layer. This approach enables an efficient method to select 3D deposition scan-paths.

Keywords: Machine Learning; Additive Manufacturing; deposition pattern; tool-path planning; recurrent neural network

1. Introduction

Laser Aided Additive Manufacturing (LAAM), also termed Laser Metal Deposition (LMD), Directed Energy Deposition (DED), utilizes a high-powered laser beam to melt blown powder jets or wire feedstock for metallic additive manufacturing. LAAM can be used for 2D materials processing such as surface cladding (Naghiyan Fesharaki, Shoja-Razavi et al. 2018) and surface alloying process. Developments in tool-path generation and process studies extends the application to 3D processing such as repair (Zhang, Li et al. 2018) of part with simple geometry and progressively in 3D printing parts with increasing geometric complexities (Ding, Dwivedi et al. 2017).

* Corresponding author. Tel.: +65-961-732-72;
E-mail address: chewyx@simtech.a-star.edu.sg.

The flexibility of this technology to use different laser beam size, laser power and material feeding rate, gives the potential to perform 3D printing at higher deposition rates (Herzog, Seyda et al. 2016) compared to other powder-bed AM processes.

The higher heat input required with increasing build rate can readily lead to localized heat accumulation, especially for parts with small foot-print in the x-y plane (z-direction is in vertical direction). The clad dimensions and microstructure is determined by the melt-pool thermal gradient and solidifications rates (Song, Chew et al. 2018). Thus, heat accumulation implies lower stability and consistency in these two parameters within the same layer and more so with increasing deposited layers. Regions with lower bead height may be out of the powder focus position (for blown powder delivery method), yielding a lower than expected build height. During the next layer, the powder focus position will be further way, accumulating more differences in height deviation. For 3D printing process, the toolpath is usually pre-programmed without in-situ correction or feedback to modify the powder nozzle position. When height deviation within the layer becomes significant, printing of the next layer is unable to continue without intervention to make rectifications.

One method to improve consistency in the deposited height includes online-feedback control of the laser power (Bi, Gasser et al. 2006). However, this will involve other technical challenges pertaining to hardware integration and accurate melt-pool characteristics or temperature monitoring. In this work, it is proposed to study laser deposition patterns to determine the optimized deposition strategy to improve process stability and consistency in layer height. The laser scanning pattern which gives the most homogenized temperature distribution is used as a selection criteria. An integrated finite element (FE) numerical and machine learning model is proposed for more efficient evaluation of the deposition pathways. This combined prediction model aims to address the huge computational time required when simulating multi-layer deposition processes. Most numerical models focused on simulating single or multi-beads depositions (Chew, Pang et al. 2015, Heigel, Michaleris et al. 2015) investigating only specific physical phenomenon and fields due to the complexities of the LAAM process. Scaling up the numerical simulation for longer process time in 3D printing with consideration of deposition patterns will cause an exponential increase in computation time. Alternatively, experimental studies may also be performed for toolpath optimization (Angelastro, Campanelli et al. 2017), but numerical model may be able to provide further useful insights to understanding the underlying mechanisms from analyzing the generated data.

In this work, i) the thermal fields of eight variants of the basic raster scan zig-zag pattern were analyzed for deposition of a cube with five AM layers. The FE numerical model used to compute the temperature evolution had been developed and reported in an earlier work (Ren, Chew et al. 2019). ii) The temperature field results of the first five layers were used to train a Temperature-Pattern Recurrent Neural Networks (TP-RNN). The trained machine learning algorithm (TP-RNN) is then applied to predict temperature fields of the $(n+1)^{th}$ layer based on numerical results of the $(n-1)^{th}$ and n^{th} layers. iii) A selection evaluation criteria reported in (Ren, Chew et al. 2019) is then proposed and applied to select the optimized pattern for the machine learning output of the $(n+1)^{th}$ layer. The optimized toolpath is recomputed using the FE model for input data for propagation to the next layer. With this approach, the optimized laser scanning patterns for multi-layer LAAM process can be determined.

2. Methodology

The details on the laser scanning patterns evaluated for multi-layer cube deposition is elaborated in this section. The first step involves computing all the possible permutations of the selected variants of the scanning patterns for the first few layers to obtain the thermal field evolution. An inter-layer TP-RNN model is then introduced to describe the connection between temperature fields in adjacent depositing layers and

selected laser scanning pattern. Finally, the multi-layer cube laser scanning pattern planning framework is proposed to improve the homogeneity of the temperature distribution by choosing an appropriate laser scanning pattern strategy.

2.1. Multi-layer LAAM simulation plan

A five-layer cube was designed to be deposited at the center of a 5mm thickness substrate for the simulation experiment. The zigzag scanning patterns selected to build the part, consists of eight variants, with each starting from the four individual corner points (A, B, C and D) and scanning along two directions (x-direction and y-direction), which are referred as XA, XB, XC, XD, YA, YB, YC and YD respectively. The schematic of the experiment design is shown in Fig 1.

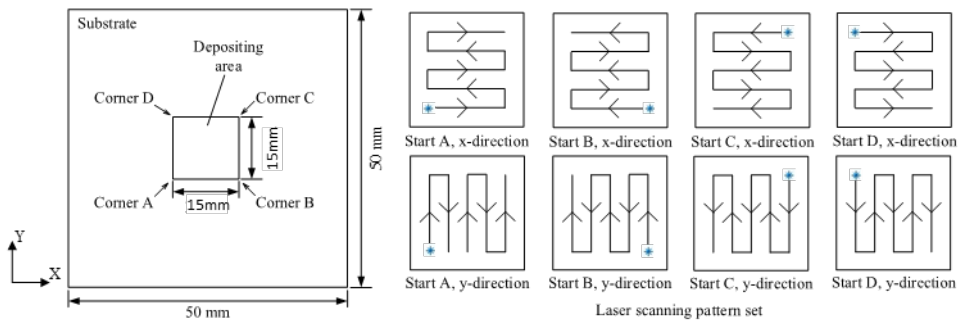

Fig. 1. Simulation experiment design with laser scanning pattern set. * indicates the laser scanning starting point.

It is observed from empirical experience that the scanning direction should generally be perpendicular in adjacent layers when Zigzag scanning pattern is used, thus the laser scanning direction is set along x-direction for odd layers and y-direction for even layers. Based on the discussed consideration, each scanning pattern used in the current layer can lead to four different selections in the next layer. In the experiment, the XA is selected for the first layer, followed by 4 possible selections for the second layer, and 16 possibilities for the third layer and so on. The propagation of the laser scanning pattern for different layers is shown in the Fig 2.

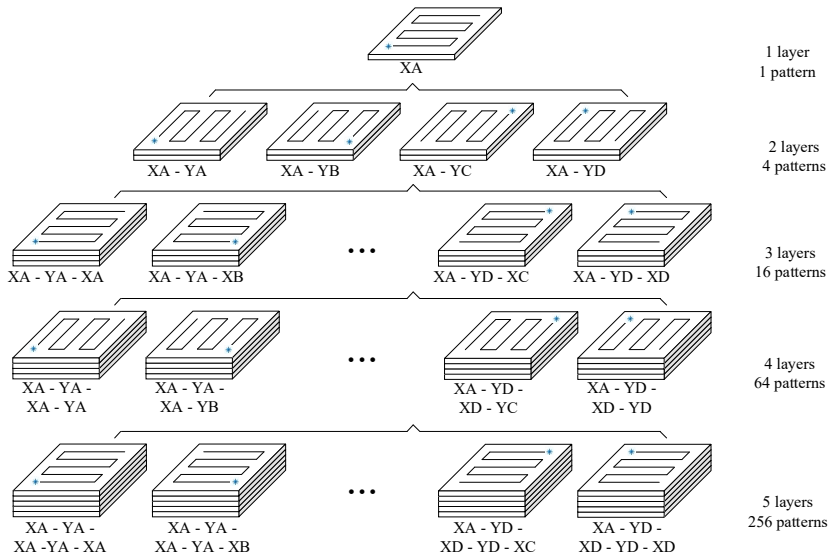

Fig. 2. Laser scanning strategies for first few layers (XA - YA - XA - YA - XA indicates the XA, YA, XA, YA and XA are selected as laser scanning pattern for first to fifth layers respectively).

LAAM related process parameters used in the simulation are given in Table 1. Using a 50 % overlap for deposition processes, the geometry of the unit domain in simulation is modified based on experimental calibration and given as $1.1\times1.1\times0.5$ mm^3.

Table 1. Process parameters used in the proposed integrated model

Laser related parameters	Laser beam radius r	1×10^{-3} m
	Initial laser power P	1.07×10^{3} W
	Laser scanning speed v	2×10^{-2} m/s
	Laser absorptivity	0.42 (Song, Chew et al. 2018)
Material related parameters	Material properties	Stainless steel 316
	Powder flow rate	16.6 g/min
	Powder absorption rate	50% (Chew, Pang et al. 2015)
	Powder initial temperature	1723 K
	Overlap rate	50%
Substrate related parameters	Substrate initial temperature	293 K

2.2. Inter-layer temperature field prediction algorithm

It is evident that the number of the laser scanning strategies increases exponentially with the increase of the depositing layers, making it immensely challenge to simulate every possible case and then select an appropriate one. Thus, this section illustrates the method used to efficiently consider the different cases. Under the condition of a constant process parameters, the machine learning algorithm predicts temperature field of the next layer using numerical results of current and previous layers. Using P_i for the laser scanning

pattern in layer i and T_i for temperature field for layer i after deposition, the proposed function can be described as $f(T_i, T_{i-1}, P_{i+1}) \rightarrow T_{i+1}$.

To normalize the temperature field generated by different dimensional cube, a feature extraction method is used to form a 10×10 matrix $\boldsymbol{T}_{\boldsymbol{tem}}^{\boldsymbol{i}}$ to describe T_i. Each layer is decomposed into 10×10 blocks $b_{m,n}$ (m, n ∈ [1,10]), the element $t_{m,n}$ (m, n ∈ [1,10]) in the matrix T_i represents the mean temperature in the block $b_{m,n}$. In the simulation, the temperature field is exported via a uniform mesh where unit cell is 0.1×0.1×h mm^3 (h is the thickness of one layer). The number of temperature nodes in each block depends on the dimension of the depositing cube. The value of $t_{m,n}$ is computed by averaging the temperature of all the nodes in the block $b_{m,n}$. The discretization of one-layer temperature field is illustrated in Fig 3.

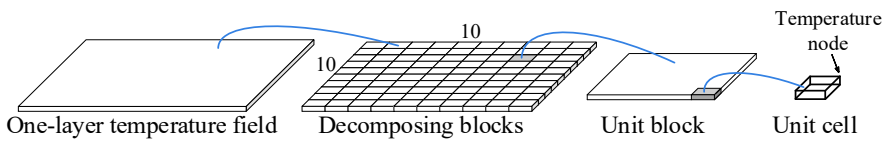

Fig. 3. Discretization of temperature field map from numerical model to matrix input data for machine learning

The temperature field matrix of the first layer $\boldsymbol{T}_{\boldsymbol{tem}}^{\boldsymbol{1}}$ deposited with laser scanning pattern $P_{pattern}$ (pattern ∈ (XA, XB, XC, XD, YA, YB, YC and YD)) also serves as matrix $T_{pattern}$ to describe the laser scanning pattern $P_{pattern}$. The function $f(T_i, T_{i-1}, P_{i+1}) \rightarrow T_{i+1}$ thus can be described as $\boldsymbol{f}\left(\boldsymbol{T}_{\boldsymbol{tem}}^{\boldsymbol{i-1}}, \boldsymbol{T}_{\boldsymbol{tem}}^{\boldsymbol{i}}, \boldsymbol{T}_{\boldsymbol{pattern}}^{\boldsymbol{i+1}}\right) \rightarrow \boldsymbol{T}_{\boldsymbol{tem}}^{\boldsymbol{i+1}}$. An TP-RNN model structure is designed to represent the function f. Besides the input layer and the output layer, the structure also contains an RNN hidden layer with 500 LSTM cells and a fully connected layer with 200 neurons, as shown in Fig 4.

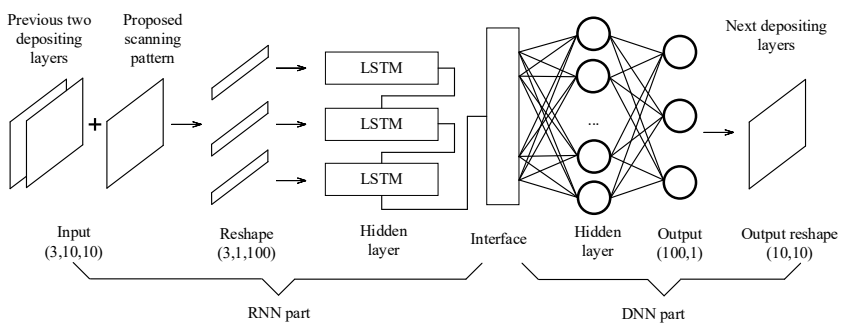

Fig. 4. RNN-DNN model structure for the machine learning algorithm

The number of laser scanning patterns for depositing n layers is 4^{n-1}. Therefore, this integrated finite element and machine learning model only requires the numerical simulation to perform 'n' number of simulation runs for building 'n' layers instead of 4^{n-1} simulation runs when considering all the possible permutations to select the optimal laser scanning pattern. The appropriate laser scanning pattern should be able to minimize the temperature distribution variance in each layer. The process parameters and materials properties are first imported to define the boundary and initial conditions in the numerical model. The laser scanning pattern for the first depositing layer is predefined to determine the simulation domain activation sequence. When one layer deposition simulation is completed, the temperature field for the next depositing layer is predicted via the RNN-DNN (Recurrent Neural Network-Deep Neural Network) model based on the

temperature field of deposited layer and potential laser scanning patterns. The outcome temperature field matrix T_{tem}^{i+1} are compared by calculating the temperature distribution variance. The laser scanning pattern providing the least variance would be selected for depositing the next layer. When the entire deposition simulation is completed, the selected laser scanning paths for each layer is the final output.

The rectified linear unit (ReLU) is selected as the activation function in the neural network. The normalized mean square error (nMSE) is chosen as the evaluation metric as defined in Eq. (1), where y_i is the ground truth temperature field matrix and y_i^* is the predict temperature field matrix. The parameters of the model is optimized using Adaptive Moment Estimation (Adam) by back propagating the error at the output layer, as Adam updates adaptive learning rates for each parameter (Ruder 2016). In data preprocessing phase, the data was split into the training set and test set according to the ratio of 9:1.

$$nMSE = \frac{1}{n}\sum_{i=1}^{n}(y_i - y_i^*)^2 \quad (1)$$

The nMSE on the training test and accuracy on the test set were recorded every epoch, where the accuracy is given in Eq. (2). The nMSE value decreases from over 100,000 to below 20,000 after 500 epochs while accuracy increases till over 90% after 100 epochs and 95.05% after 1000 epoch. The convergence suggest that the RNN-DNN model is able to fit the function f well.

$$Accuracy = \frac{1}{n}\sum_{i=1}^{n}\frac{\|y_i - y_i^*\|}{y_i} \times 100\ \% \quad (2)$$

3. LAAM Simulation and Prediction Results

The thermal history graphs prediction for the multi-layers deposition stimulations are illustrated in Fig. 5 for the case where every layer starts from the same location. From the temperature distribution at the time instance where the deposition ends for each layer, it is observed that the extent of heat accumulation increases with increasing layers. The integrated model will attempt to optimized and minimize the heat accumulation effect.

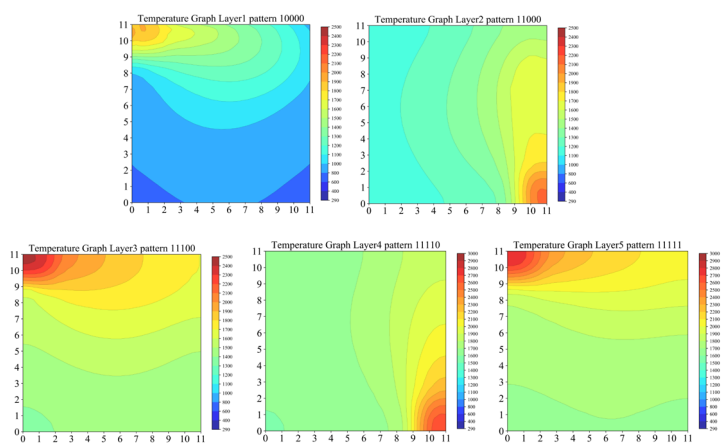

Fig. 5. Heat accumulation for scan paths which starts at same location for each layer.

To evaluate the proposed LAAM multi-layer scanning pattern planning frame, a 10-layer cube of SS316 is designed to be deposited at the center of a 5mm thickness substrate, as shown in left of Fig 1 above. The laser scanning pattern for the first layer is selected as XA. The laser scanning pattern selected using the integrated model is given in Table 2. It can be found that temperature distribution variance of the whole component decreases along with the increase of the deposition layers. Another observation is the suggested optimized starting point for the adjacent layers is located diagonally across the deposition area. This selection of raster scan starting points will help to increase the homogeneity of the temperature distribution of the printed part. In addition, it was also observed that the difference between the resulting temperature variance for different scanning patterns reduces with increasing deposition area. This is because the part has heated up considerably and cooling rate has reduced, causing slowly heat dissipation from the deposited layer. Hence, the effect of scanning pattern diminishes. At this point, another methods are required to reduce the heat accumulation for example, reducing laser power or allowing the part to cool down. The melt-pool size for 5 layers deposition using the scanning pattern with the same starting point compared with the optimized scanning pattern is shown in Fig 6 below. It is observed that the melt-pool size can be reduced when the optimized scanning pattern is applied.

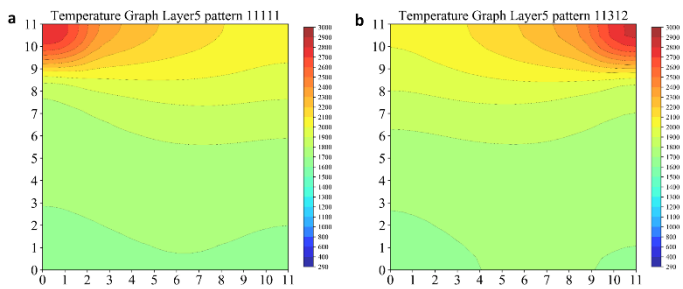

Fig. 6. a) Thermal distribution for scanning pattern starting at position A for every layer and b) thermal distribution of optimized laser scanning pattern.

Table 2. Laser scanning pattern and temperature distribution variance parameter.

	Temperature distribution variance for next layer with different start point				Selected pattern
	Start at A	Start at B	Start at C	Start at D	
Layer 2	160678.87	219906.78	186866.37	189526.36	YA
Layer 3	196223.83	170150.00	169042.44	198204.41	XC
Layer 4	108212.98	120929.94	128939.20	131719.36	YA
Layer 5	106637.94	89879.52	93015.91	113621.02	XB
Layer 6	47899.17	65012.92	53851.36	57207.22	YA
Layer 7	66406.88	56727.36	56149.50	68143.32	XC
Layer 8	43276.40	47019.70	50928.71	53603.76	YA
Layer 9	43329.99	36833.33	36165.46	45151.60	XC
Layer 10	30096.93	32648.92	35599.72	37955.91	YA

4. Conclusion

In the simulation evaluation, a five-layer cube is designed to be deposited on the center of the square substrate with 256 different laser scanning strategies. From this work, it is demonstrated that the integrated finite element and machine learning approach allow an efficient approach to go through all the possible

scanning pattern and select the one which enable a more homogeneous temperature distribution. The trained TP-RNN model is able to take temperature field of the current and previous numerical results thermal field as input and then predicts the temperature field of the next layer as output. Using the predicted output from the TP-RNN model, the optimized pattern for the next layer is selected and iteration to next layer continues. In addition, the developed TP-RNN model is able to fit the temperature field – laser scanning pattern function well. From the comparison of the size of the thermal contour around the melt-pool after 5 layers, it can be observed that the optimized scanning pattern resulted in less heat accumulation around the melt-pool. As each layer is deposited, the effect on scanning pattern reduces as cooling rate reduces. In future work, the relative size between printed area and substrate, as well as laser power will be investigated to understand how these parameters affects selection of laser scan paths.

Acknowledgements

This research was supported by Agency for Science, Technology and Research (A*Star), Republic of Singapore, under the IAF-PP program “Integrated large format hybrid manufacturing using wire-fed and powder-blown technology for LAAM process”, Grant No: A1893a0031.

References

Naghiyan Fesharaki, M., R. Shoja-Razavi, H. A. Mansouri and H. Jamali (2018). "Microstructure investigation of Inconel 625 coating obtained by laser cladding and TIG cladding methods." Surface and Coatings Technology 353: 25-31.

Zhang, X., W. Li, X. Chen, W. Cui and F. Liou (2018). "Evaluation of component repair using direct metal deposition from scanned data." The International Journal of Advanced Manufacturing Technology 95(9): 3335-3348.

Ding, Y., R. Dwivedi and R. Kovacevic (2017). "Process planning for 8-axis robotized laser-based direct metal deposition system: A case on building revolved part." Robotics and Computer-Integrated Manufacturing 44: 67-76.

Herzog, D., V. Seyda, E. Wycisk and C. Emmelmann (2016). "Additive manufacturing of metals." Acta Materialia 117: 371-392.

Song, J., Y. Chew, G. Bi, X. Yao, B. Zhang, J. Bai and S. K. Moon (2018). "Numerical and experimental study of laser aided additive manufacturing for melt-pool profile and grain orientation analysis." Materials & Design 137: 286-297.

Bi, G., A. Gasser, K. Wissenbach, A. Drenker and R. Poprawe (2006). "Investigation on the direct laser metallic powder deposition process via temperature measurement." Applied Surface Science 253(3): 1411-1416.

Chew, Y., J. H. L. Pang, G. Bi and B. Song (2015). "Thermo-mechanical model for simulating laser cladding induced residual stresses with single and multiple clad beads." Journal of Materials Processing Technology 224: 89-101.

Heigel, J. C., P. Michaleris and E. W. Reutzel (2015). "Thermo-mechanical model development and validation of directed energy deposition additive manufacturing of Ti–6Al–4V." Additive Manufacturing 5: 9-19.

Angelastro, A., S. L. Campanelli and G. Casalino (2017). "Statistical analysis and optimization of direct metal laser deposition of 227-F Colmonoy nickel alloy." Optics & Laser Technology 94: 138-145.

Ren, K., Y. Chew, J. Y. H. Fuh, Y. F. Zhang and G. J. Bi (2019). "Thermo-mechanical analyses for optimized path planning in laser aided additive manufacturing processes." Materials & Design 162: 80-93.

Ren, K., Y. Chew, Y. F. Zhang, G. J. Bi and J. Y. H. Fuh (2019). "Thermal analyses for optimal scanning pattern evaluation in laser aided additive manufacturing." Journal of Materials Processing Technology 271: 178-188.

Ruder, S. (2016). "An overview of gradient descent optimization algorithms." arXiv preprint arXiv:1609.04747.